Multistep optimization of a cell-penetrating peptide towards its antimicrobial activity

Marco Drexelius[1], Andre Reinhardt[1], Joshua Grabeck[1], Tom Cronenberg[2], Frank Nitsche[3], Pitter F. Huesgen[1,4,5], Berenike Maier[2], Ines Neundorf[1*]

[1]Institute for Biochemistry, Department of Chemistry, Faculty of Mathematics and Natural Sciences, University of Cologne, Zuelpicher Str. 47a, 50674 Cologne, Germany

[2]Institute for Biological Physics, Department of Physics, Faculty of Mathematics and Natural Sciences, University of Cologne, Zuelpicher Str. 47a, 50674 Cologne, Germany

[3]Institute for Zoology, Department of Biology, Faculty of Mathematics and Natural Sciences, University of Cologne, Zuelpicher Str. 47b, 50674 Cologne, Germany

[4]Central Institute for Engineering, Electronics and Analytics (ZEA-3), Forschungs-zentrum Jülich, Jülich, Germany

[5]Cologne Excellence Cluster on Cellular Stress Responses in Aging Associated Diseases (CECAD), Medical Faculty and University Hospital, University of Cologne, Cologne, Germany

*Corresponding author: Prof. Dr. Ines Neundorf, phone: (+49) 221 4708847, University of Cologne, Cologne, Germany, ines.neundorf@uni-koeln.de

Keywords

Antimicrobial peptides; cell-penetrating peptides; antimicrobial activity; membrane-activity; anticancer peptides

Abstract

Multidrug resistant (MDR) bacteria have adapted to most clinical antibiotics and are a growing threat to human health. One promising type of candidates for the everlasting demand of new antibiotic compounds constitute antimicrobial peptides (AMPs). These peptides act against different types of microbes by permeabilizing pathogen cell membranes, whereas being harmless to mammalian cells. Contrarily, another class of membrane-active peptides, namely cell-penetrating peptides (CPPs), is known to translocate in eukaryotic cells without substantially affecting the cell membrane. Since CPPs and AMPs share several physicochemical characteristics, we hypothesized if we can rationally direct the activity of a CPP towards antimicrobial activity. Herein, we describe the screening of a synthetic library, based on the CPP sC18, including structure-based design to identify the active residues within a CPP sequence and to discover novel AMPs with high activity. Peptides with increased hydrophobicity were tested against various bacterial strains, and hits were further optimized leading to four generations of peptides, with the last also comprising

fluorinated amino acid building blocks. Interestingly, beside strong antibacterial activities, we also detected activity in cancer cells, while non-cancerous cells remained unharmed. The results highlight our new candidates, particularly those from generation 4, as a valuable and promising source for the development of future therapeutics with antibacterial activity and beyond.

Introduction

Since the discovery of arsphenamine (also known as Salvarsan) by Paul Ehrlich in 1907 [1], and later on of penicillin by Alexander Fleming in 1928 [2], the number of antibiotics as well as their use for treatments in different areas, such as agriculture [3], human and veterinary medicine [4], has steadily increased. As a result of this over usage resistances in bacteria evolved and have more and more become a real global threat, demanding for the development of novel antibiotics with improved activity spectra to counter the development of multidrug resistant strains [5,6]. During the past years, great efforts have been made in this direction leading, for instance, to the discovery of the macrolide azithromycin [7], or the cephalosporine ceftriaxone [8]. Both antibiotics are effective against many bacteria used as clinical standards but meanwhile also face the problem that bacteria find a way to adapt to them [9].

A novel potential class of antibiotics is seen in antimicrobial peptides (AMPs), a structurally highly diverse group of peptides that kill bacteria mainly by membrane permeabilization [10]. This mechanism is supported by their structural properties including a usually high content of positively charged, as well as hydrophobic amino acid residues [11]. These two types of amino acids are often orientated along two faces within different kinds of secondary structures, like alpha helices [12] or beta sheets [13], promoting a more basic, charged face and a nonpolar face. The positively charged side of the peptides perfectly interacts with negatively charged components at the outer surface of bacterial membranes, while hydrophobic interactions of the other face enhance insertion of the peptide into the hydrophobic core of the lipid bilayer [14,15]. Further on, this leads to several membrane perturbating mechanisms finally ending in membrane lysis and cell death. However, some AMPs are able to internalize and infiltrate bacteria, too. Following they may inhibit distinct steps of metabolic processes, such as nucleic acid or protein synthesis [16,17].

Naturally occurring AMPs are found in all domains of live where they act as a first line biologic defense against pathogens, like bacteria, viruses [18], fungi [19] or other

parasites [20]. Examples include Magainin isolated from African clawed frog [21] or cationic antimicrobial peptide CAP18 obtained from rabbits [22]. Until today, the set of natural AMPs is complemented by synthetically derived peptide sequences that share the advantage of chemical modification [23]. Interestingly, many antimicrobial peptides exhibit anti-cancer activity, and indeed, such anti-cancer peptides (ACPs) may provide a promising, new approach in chemotherapy [24,25]. ACPs are usually cationic and therefore, attracted by the more negatively charged cell membrane of cancerous cells [26,27].

Within this work, we aimed to modify the sequence of the cell-penetrating peptide sC18 [28], and to change its activity to act as an AMP. sC18 is a *C*-terminal fragment of the cationic antimicrobial peptide CAP18, which, for itself, exhibits only very moderate antimicrobial activity. In recent work, we developed sC18 as a very effective transporter for various cargos, e.g. metal organic complexes [29], cytostatic drugs [30], or peptides [31]. From our previous studies, we have also recognized that sC18 forms an amphipathic alpha-helical structure when in presence of a lipid environment [30]. Since CPPs and AMPs act differently to certain organisms (e.g. mammalian cells, or bacteria), but often share common physicochemical characteristics [32], we wondered if we could switch the activity of sC18 to become an AMP. Moreover, the development of AMPs based on CPP structures, from which it is already known that they are non-toxic, might be beneficial in terms of safe application.

Previously, it was reported that an increase in the amount of hydrophobic amino acids led not only to increased antibacterial activity [33], but also to an enhanced overall selectivity between bacteria and mammalian host cells [34]. Further options to improve such properties were seen in the incorporation of unnatural amino acids that further increase stability against enzymatic hydrolysis [23,35]. Thus, within this work, we run several cycles of evolution on the structure of sC18, including rational amino acid displacement with hydrophobic and/or unnatural amino acids, to yield more stable and more selective and still highly active new antimicrobial peptides.

Materials and methods

Materials

Chemicals, reagents and consumables, which were used during this work, were obtained from Fluka (Taufkirchen, Germany), Merck (Darmstadt, Germany), Sarstedt

(Nümbrecht, Germany), Sigma-Aldrich (Taufkirchen, Germany) and VWR (Darmstadt, Germany). Nα-Fmoc protected amino acids were purchased from Iris Biotech (Marktredwitz, Germany). Protection groups for the trifunctional amino acids were Pbf (Arg), Trt (Asn, Gln, His, Cys), Boc (Trp, Lys) and *tert*-butyl (Asp, Glu, Ser, Thr, Tyr). Purified red blood cells (SER-10MLRBC) were ordered from zenbio (ResearchTriangle Park, NC 27709, USA) via the German distributor biocat (Heidelberg).

Used bacterial strains: *Bacillus subtilis* (ATTC 6633), *Corynebacterium glutamicum* (ATCC 13032), *Escherichia coli* K12 (MG 1625), *Micrococcus luteus* (DSM 20030), *Mycobacterium phlei* (DSM 48214), *Salmonella typhimurium* (TA 100), *Pseudomonas fluorescens* (DSM 50090) and *Pseudomonas aeruginosa* (PA14).

Peptide synthesis

Peptides were synthesized using orthogonal Fmoc/*t*Bu strategy on Rinkamide resin (loading 0.48 mmol/g, 0.015 mmol scale). Amino acid coupling was realized using an automated peptide synthesizer from MultiSynTech and following double coupling steps with 8 equivalents (eq.) Fmoc-aa-OH, Oxyma pure® and DIC. Fmoc-protecting group was removed with piperidine (20 % in DMF). 5,6-carboxyfluorescein (CF)-labeled peptides were synthesized according to Ref. [31]. Peptides were labeled at the *N*-terminus with CF. Finally, peptides were removed from the resin using TFA/TIS/H2O (95:2.5:2.5 v/v/v) for 3 h and precipitated in ice-cold diethyl ether. Peptides were purified using preparative RP-HPLC, and fractions were analyzed by analytical RP-HPLC ESI-MS. Final purity of all compounds was >95 % (see also Figures S5-S7).

Circular dichroism (CD) spectroscopy

Peptides were dissolved in 10 mM phosphate buffer (pH 7) or 10 mM phosphate buffer (pH 7) with the addition of trifluoroethanol (TFE) (1:1) to yield a concentration of 20 µM. Spectra were accorded from 180 to 260 nm in a 1 mm thick quartz cuvette. Conversion of θ measured in degree to the characteristic θ for the peptide was realized by using the following equation:

$$\theta = \frac{\theta_{measured}}{(10 * n_{residues} * c_{peptide} * d_{cuvette})} = \frac{deg * cm^2}{dmol}$$

Antimicrobial activity assay

Bacterial cultures of an optical density of more than 0.7 at 600 nm were used. In a 96-well plate 180 µL of MH-medium, 10 µL of bacteria suspension and 10 µL of peptide solution were mixed. The resulting cultures were screened at several different peptide concentrations (as triplicates). As negative control pure water and as positive control 35% ethanol in medium were used. All samples were then incubated at 37 °C for 6 h. Afterwards, 10 µL of a 1 mg/mL solution of iodnitrotetrazolium chloride in pure DMSO was added to each well, and samples were further incubated for 30 min at 37 °C. Finally, the absorption of formazan at 560 nm in each well was measured using a plate reader. The MIC was calculated as the average of three independent experiments performed in triplicate. For *P. aeruginosa* six singular experiments were performed.

Proteolytic digestion

100 µM peptide solutions in 100 mM $(NH_4)_2CO_3$ buffer were generated and incubated with 2 µM trypsin at 37 °C and shaking at 1200 rpm. At different timepoints 15 µL aliquots were taken, inactivated with the addition of 45 µL formic acid (10%) and stored at -18 °C. After thawing for analysis, samples were diluted in LC-MS buffer (10 % acetonitrile, 0.1 % formic acid, 90% water) and measured by LC-MS (Agilent 1600 series and LTQ-XL, Thermo, mass spectrometer).

To test the stability in culture supernatant, bacterial cultures of an optical density of more than 0.7 at 600 nm were used. The bacterial culture was centrifuged, and the supernatant gathered for further experiments. 200 µL peptide solutions of 4 x MIC (regarding the used bacterium) were prepared in culture supernatant and incubated overnight. As control, a solution of medium only was used. The next day, peptide solutions were diluted 1:3 in fresh medium and an antibacterial assay was performed as already described. As control, peptide samples pretreated with growth medium only were used.

Hemolysis assay

Human red blood cells (*hRBCs*) (zenbio, USA) were washed in PBS buffer and centrifuged (3,000 x g, 4 °C, 5 min) four times. The cells were diluted with PBS to a concentration of 5 % (v/v) and 100 µL of this suspension were given in each well of a 96 well plate with either 50 µL peptide solutions in PBS or 10 % Triton X-100 in PBS as positive control. After 1 h or 24 h incubation at 37 °C, the plate was centrifuged

(2,500 x g, 3 min) and 100 µL supernatant of each well were transferred to another well plate. The absorption of these solutions at 560 nm was measured with a plate reader to determine the hemoglobin concentration.

Cytotoxicity assay

HeLa (20,000), MCF-7 (15,000) or HEK293 (15,000) cells were seeded in a 96 well plate. The plate was incubated overnight for HeLa/MCF-7, or for 48 h when using HEK293 cells, at 37 °C with 5 % CO_2. Afterwards, cells were treated with 100 µL peptide solutions in medium, or with 100 µL ethanol (70 %) as positive control. These samples were incubated for 24 h, then cells were washed two times with PBS. 100 µL 10 % resazurin solution in respective medium were given to each well for 1 h at 37 °C. The resorufin fluorescence was measured by using a microtiter plate reader (excitation: 550 nm, emission: 595 nm) to determine cellular survival.

Lactate dehydrogenase (LDH) release assay

The CytoTox-One™ Homogeneous Membrane Integrity Assay by Promega was used for this experiment according to the manual's instructions. Briefly, cell medium was mixed with cell suspension in a dark 96 well plate leading to 17.000 *HeLa* cells in 200 µL. The plate was incubated at 37 °C with 5 % CO_2. The next day, cells were treated with 100 µL peptide solutions. After incubation for 1 h at 37 °C, the plate was equilibrated at room temperature for 20 min before lysis buffer was added to obtain positive controls. CytoTox-One™ reagent was added to each of the wells and the measurement of fluorescence was done using a microtiter plate reader (excitation: 560 nm, emission: 590 nm).

Flow cytometry

For quantifying cellular uptake 100,000 HeLa or HEK293 cells, respectively, were incubated overnight at 37 °C with 5 % CO_2 in a 24 well plate. Afterwards, the supernatant was removed, and cells were incubated with 400 µL CF-labeled peptide solutions (5 or 10 µM) in medium without FBS for 30 min at 37 °C. Then, cells were washed two times with 500 µL PBS, following addition of 150 µL trypsin. After 5 minutes incubation at 37 °C, cells were resuspended in 850 µL of colorless medium with FBS. 100 µL of each solution were transferred in a 96 well plate and cellular uptake was determined with the Guava® easyCyte HT™ System (Merck) using the

GRN-B (525/30) channel, counting 10,000 cells per well. Results were normalized to the uptake of sC18 and calculation of significances were done using Microsoft excel t-test function, to determine the significances of two different datasets. The fluorescence spectra measured were also visualized with Kaluza analysis version 2.1 software.

Scanning electron microscopy (SEM)

Bacteria were cultured as previously described. 270 µL aliquots were taken from each culture and treated with 30 µL peptide solution to have a final concentration of 4 x MIC. All samples were incubated for 90 min; water served as control sample. After incubation, samples were centrifuged (5,000 rpm, 10 min, 4 °C) and washed twice with 100 µL PBS buffer following centrifugation. The cell pellets were fixed with 2.5 % glutaraldehyde in PBS for 30 min and afterwards dehydrated with ethanol solutions of increasing concentrations (30, 50, 70, 80, 90, 99 %). Cell pellets were then transferred to hexamethyldisilazane (HMDS)/ethanol (1:1) for 10 min followed by 100 % HMDS for another 10 min as a substitute for critical point drying. Afterwards they were allowed to fall dry, mounted on sample holders and sputter coated with 12nm gold. Samples were analyzed using a FEI Quantum 250 FEG scanning electron microscopy.

Results and discussion

Stepwise AMP design by sequence-based refinement of sC18

Inspired by the work of Süssmuth et al. [36], we systematically replaced specific amino acids in the sequence of sC18 with hydrophobic ones. Aim was to increase the general hydrophobicity of the peptide, which was already shown to be a promising way of enhancing antimicrobial activity [33,36]. As it is assumed that membrane active peptides use a mechanism of coiling into a double-faced alpha helix to interact with the cell membranes [37], we first carefully inspected the helical wheel projection of sC18. From this we suspected three positions to have an exceptional effect. For instance, it can be appreciated that substitution of position Arg10 and Lys16 might be favorable, since this enlarges the hydrophobic face of the amphipathic helix (Figure 1, Figure S1). On the other side, substituting position Glu15 eliminates the negative charge delivered by glutamate that would otherwise inhibit the interaction of the positively charged amino acid residues with negatively charged compounds at the

outer surface of the plasma membrane. Indeed, we have recently observed such an effect in terms of the cell-penetrating activity of sC18, when we replaced Glu15 by alanine [38], further indicating improved membrane interaction after elimination of the negative charge.

To prove our hypothesis, we performed an isoleucine scan of sC18 to find out how substitution with a single hydrophobic amino acid would influence the AMP activity of sC18, resulting in the first generation of novel possible AMPs **1a**-**1o** (Table 1). All peptides were synthesized by Fmoc-based solid phase peptide synthesis strategy.

TABLE 1

The new peptides **1a**-**1o** were tested in a first screen by incubating different gram-positive (*B. subtilis*, *M. luteus*) and gram-negative (*P. fluorescens*) bacteria for 6 h with two different peptide concentrations (Figure 1). As expected from the helical wheel projections, the results showed increased antimicrobial activity especially for exchanges at position Arg10 (**1j**), Glu15 (**1n**) and Lys16 (**1o**). As a consequence, we concluded that these positions represent important nodes within the sC18 sequence.

FIGURE 1

Therefore, we further tested the impact of these positions on AMP activity analyzing double and triple isoleucine mutants **2a**-**2d** (Table 1). The new peptides were investigated in comparison to the former generated peptides **1j**, **1n** and **1o** using a panel of different bacterial strains, including gram-positive *B. subtilis*, *C. glutamicum* and *M. luteus*, gram-negative *P. fluorescens*, *E. coli* and *S. typhimurium*, and the acid-fast bacterium *M. phlei* (Figure 2A and Figure S2, for MIC_{50} values see Table 2). To get more insights into the membrane-activity of the herein tested peptides, the different bacterial strains were chosen according to their differences in cell-wall composition and organization.

FIGURE 2

We observed almost no antimicrobial effect when the peptides were in presence of *E. coli* or *M. phlei* (Figure S2). *M. phlei* represents an acid-fast bacterium and is characterized by an additional outer mycolic acid layer what might explain this observation [39]. *E. coli* is reported to have an increased outer membrane rigidity, which is a result of acylated lipids and might prevent AMP interaction [40]. However, for two other gram-negative bacteria (*P. fluorescens* and *S. typhimurium*), as well as the other bacterial strains tested, considerable activities with MIC_{50} values in the lower micromolar range were detected. Summarizing, it seems that an extension of the

hydrophobic face within the helix is more effective than the simple deletion of the glutamic acid in position 15, since this peptide **1n** displayed less activity, compared to **1j** and **1o**. On the other hand, all double and triple mutants exhibited a general higher AMP activity than the mono-substituted versions guiding us to the design of the next generation of peptides.

Here, we aimed at improving peptide potency by incorporating phenylalanine as an even more hydrophobic amino acid. In addition to the mutants bearing single exchanges at positions Arg10, Glu15 and Lys16 (**3a**-**3c**), we directly generated the double and triple mutated variants (**3d**-**3g**) (Table 1 and Figures S7, S8). All peptides were analyzed concerning their antibacterial activity as described before for the Ile mutants (Figure 2B and Figure S3). Peptides **3f** and **3g**, having positions 15 and 16 of sC18 substituted by phenylalanine, demonstrated the highest antimicrobial activity against all strains tested, except for *E. coli*. Of note is further that in contrast to the isoleucine peptides, all sequences of this third generation exhibited antimicrobial activity against *M. phlei*. Moreover, the results indicated that the mono variants were more active when isoleucine was present instead of phenylalanine, while the substitution at position Arg10 led to the highest increase in activity. Assumedly, position 10 was more important for the formation of a stable alpha helix, compared to position 16, and therefore, substitution with a hydrophobic amino acid gained more impact at position 10. On the other side, the double and triple mutants with phenylalanine displayed higher activities than the isoleucine versions. Therefore, we chose the phenylalanine mutants for a final, fourth, optimization cycle.

Having observed optimized activity when the negative charge at Glu15 was substituted, we removed this amino acid out of the sC18 sequence, yielding peptide **4a** that served as a control for peptides of this 4^{th} generation. Additionally, we included **4b** as an analogue to **3g**, bearing phenylalanine substitutions for Arg10 and Lys15. In a further attempt to optimize the parent sequence, we increased the hydrophobicity even more by introducing fluorinated amino acids. As fluorination was reported to lead to minimal steric alterations [41], we used the mono-, di- and pentafluorinated phenylalanine variants X_1-X_3 (Table 1 and Figure S8, S9) and replaced the same positions as in **4b**, yielding peptides **4c**-**4e**. Again, all novel peptide variants were obtained in high purities and directly evaluated concerning their biological activity as described before. Our results showed that the antimicrobial activity of **4a**, in comparison to sC18, was slightly increased against *C. glutamicum*

and *P. fluorescens* (Table 2 and Figures 2c and S4, S5), while **4b** exhibited even better activity, comparable to former peptide **3g**. This result let us conclude that the elimination of the negative charge seemed to greatly affect the antimicrobial activity in a positive way, while the additional present increased hydrophobicity in **4b** even strengthened the formation of a secondary structure. Notably, we could verify this assumption when analyzing peptides **3a**-**3g** and **4a**-**4e** by circular dichroism (CD) spectroscopy. The formation of an alpha-helical structure was clearly visible for all peptides when in hydrophobic environment (realized by the addition of trifluoroethanol, TFE) (Figure S10). Indeed, the formation of alpha helices at the bacterial membrane is known to promote the antimicrobial activity of AMPs [42]. From the obtained CD data, we concluded that our novel peptides assumedly form such stabilized secondary structures when in contact with bacteria. Moreover, the calculated hydrophobicity and hydrophobic moment of all new peptides (Table 1), but especially that of generation **3** and **4** peptides fit very well to the activities observed, and are probably a first hint linking an increase in overall hydrophobicity and formation of an amphipathic helix to enhanced membrane-activity. Of note was further that peptides **4c**-**4e** featured higher activities against all bacteria tested, with peptide **4e** exhibiting the lowest MIC_{50} values, compared to the other peptides investigated thus far. Interestingly, **4c**-**4e** also demonstrated a significant impact on *M. phlei* and to less extent on *E. coli* (Figure 2C and Figure S4) pointing to the high impact of the incorporated fluorinated amino acids. In Table 2 all determined MIC_{50} values are listed.

TABLE 2

Within a last and preliminary step, we have analyzed the activity of the most potent peptides **3g**, **4b** and **4e** against pathogenic *Pseudomonas aeruginosa* (Figure S6). Estimated MIC_{50} values were in the range of 9 µM for **3g**, 19 µM for **4b** and 11 µM for **4e**, thus, considerably higher than those measured for, e.g. *P. fluorescence*. However, considering that *P. aeruginosa* belongs to the group of ESKAPE pathogens that show increased resistance against various commonly used drugs and cause health-care associated infections, our findings might contribute to the development of more potent new drugs against this species.

In summary, our step-by-step rational design provided novel peptides with improved AMP activity demonstrating that a switch to antibacterial activity is possible.

However, although the MIC values are high for most of the analogues, only peptides **3g** and that out of generation **4** are likely to be good candidates as antimicrobials.

Peptide stability

One major concern for the future development of AMPs is their limited stability to proteolysis in physiological conditions [43]. Therefore, we tested the stability of the fluorinated peptide **4e**, which turned out to be the most promising AMP in our initial screens, in presence of trypsin. To compare the results, we took peptides **4a** and **4b** as control. Peptides were incubated with 1:50 (m/m) trypsin at 37 °C and samples were taken after several time points for analysis with LC-MS. Not surprisingly given the number of present lysines, all peptides were rapidly degraded by trypsin, but different major cleavage sites were visible, leading to similar products for **4b** and **4e** as well as another major degradation product for **4a** (Figure 3A). In addition, all peptides were rapidly cleaved after Arg5, and **4a** also quickly after Arg10, producing the peptide fragments LRKFR and NKIKK, respectively, that were the major products already after 10 minutes (Figure S11). Contrarily, **4b** and **4e** were mainly cleaved after Lys8, Lys12 and Lys14, leading to the two major products FFNK and FXNK after more than 1 h incubation (Figure S12-S13). Interestingly, the degradation process seemed to be a bit slower for **4e** in comparison to **4b**, possibly as a result of the incorporation of the fluorinated amino acids [35].

We next synthesized several of these fragments and tested if they retained antimicrobial activity against *B. subtilis* and *P. fluorescens* (Figure 3B). However, none of these fragments showed any significant antimicrobial activity when tested in a concentration of up to 50 µM. From this we concluded that the complete peptide sequence is needed for antimicrobial activity and that the mechanism of action must be very fast to avoid proteolytic inactivation.

Furthermore, to test the stability under more physiological conditions, we exposed the peptides **4a**, **4b** and **4e** to bacterial cell culture-conditioned supernatant and fresh medium as control. After 18h incubation in the respective media, we performed an antimicrobial activity assay by incubating the peptides for additional 6 h with *B. subtilis*. As depicted in Figure 3C, all peptides lost their activity when pre-incubated in bacterial cell culture supernatant but retained activity when pre-incubated in growth media only.

FIGURE 3

All in all, these results demonstrated that the incorporation of fluorinated amino acids resulted in different cleavage products and presumably slower cleavage at sites where the fluorinated amino acids sterically impair proteolytic substrate binding. However, all of the peptides were susceptible to fast degradation, and the shorter fragments did not exhibit significant activity. This suggests a very fast mechanism of action for the peptides to exert their antimicrobial effect.

Hemolytic activity and cytotoxic profiles in mammalian cells

In a next set of experiments, we wanted to find out how the peptides would perform in presence of mammalian host cells, as cytotoxic behavior was not uncommon for strong antimicrobial peptides [44]. We examined peptides **3a**-**3g** and **4a**-**4e**, since those seemed to have the most promising overall activities. Firstly, we assessed their hemolytic activity by using human red blood cells (hRBC), which were incubated for 1 h or 24 h, respectively, with the peptides (Figure 4 and Figure S14). Strikingly, after 24 h incubation hRBCs were nearly not affected by the peptides. Only peptides **4d** and **4e** were slightly more active and exhibited hemolytic activities of up to 15 % when incubated with hRBCs at higher concentrations of about 40 µM.

FIGURE 4

Afterwards, we determined the cytotoxicity against mammalian cells, choosing human embryonic kidney cells (HEK293) as our model for a non-cancerous cell line. Again, peptides were incubated with the cells for 24 h (Figure 5A). Our results proved that all tested peptides had only marginal effects to the viability of HEK293 cells, with **3g** and **4e**, showing detectable cytotoxicity above a concentration of 40 µM. To illustrate the selectivity of the peptides between bacterial and human non-cancerous cells, we estimated cytotoxic concentrations (CC_{100}) for the peptides against HEK293 cells and then calculated selectivity indices (Table 3). From Table 3 it can be deduced that all tested peptides affected HEK293 cells when present in at least 1.6-fold higher concentrations compared to the concentrations used to affect either *B. subtilis* or *P. fluorescence*. Importantly, the most active peptide, **4e**, displayed a selectivity index of approximately 40, offering high selectivity from bacterial to mammalian cells.

TABLE 3

Following, we were eager to know if the peptides would also display anti-cancer activity. Indeed, it has been already reported that many cationic anti-cancer peptides

originally derived from antimicrobial peptides [24]. Remarkably, this behavior is related to the surface similarities between bacterial and cancerous membranes [45]. Thus, we investigated the cytotoxicity of the peptides against HeLa (human cervical cancer) and MCF-7 (human breast cancer) cells (Figure 5B and 5C). In contrast to HEK293 cells, for both cancerous cell lines a clear toxic effect was observed when incubating them either with mutants **3d**-**3g**, or with the fluorinated peptides **4c**-**4e**. It is worth mentioning that **4b**, containing only natural phenylalanine, exhibited no toxicity to HeLa cells, but was significantly more toxic to MCF-7 cells at higher concentrations (> 20 µM), indicating further selectivity between different cancerous cell lines. In addition, peptides **3a**-**3c** and **4a** were nearly non-toxic to both tested cell lines.

FIGURE 5

Cellular uptake ability in mammalian cells

Since the AMPs of this work were developed from a CPP sequence [28], we were also interested if they were able to translocate in cells. Therefore, we incubated HEK293 and HeLa cells for 30 min with fluorescently-labeled peptides in a non-toxic concentration of 5 or 10 µM, respectively, and quantified their cellular uptake by flow cytometry.

FIGURE 6

We normalized the overall uptake to the parent CPP sC18, and from this it became clear that all investigated peptides, with the exception of **3a** and **3c**, showed higher cellular accumulations than the original CPP in both cell lines (Figure 6 and Figure S15). However, the uptake of the peptides was quite differently. For the series 3 peptides (which were tested at 10 µM), the highest accumulation in HEK293 cells was achieved by **3d** and **3g** with 32- and 50-fold increased uptake values compared to sC18. In HeLa cells the uptake was only moderately increased compared to sC18 by nearly 5- to 14-fold. On the other side, all peptides from the 4th generation (which were tested at 5 µM) showed rather similar uptake values in HeLa and HEK293 cells. In both cell lines, **4d** displayed the highest accumulation with a 21-fold and 18-fold increase in uptake in comparison to sC18, followed by **4c** and **4e** with a more than 10-fold increase in uptake. As all these peptides having the highest accumulation were also the most hydrophobic ones, we assumed a direct correlation of hydrophobicity to cellular uptake for both cell lines tested. Thus, not the overall net charge was dependent for the high uptake values, but rather a proper integration of

the peptide sequences into the hydrophobic core of the lipid bilayer. However, if their potency is also relied on targeting intracellular processes has yet to be elucidated. Interestingly, **3d**, **3e** and **3g**, accumulated significantly higher in HEK293 than HeLa cells. Only **3g** exhibited slight toxic effects when applied in higher concentration to HEK293 cells. In this case, we could therefore not correlate uptake and cytotoxicity. Instead, this observation let us conclude that particularly **3d** and **3g** should be investigated further as cell-penetrating peptides in HEK293 cells and related cell lines. All in all, the distinct uptake values might be the result of specific membrane interactions, which are most probably dependent on the different membrane compositions of both cell lines, as well as the distinct peptide sequences used [46]. In spite of this, it has been recently demonstrated that sequence motif and tail length of the hydrophilic basic phase of the helix are important determinants for successful cellular uptake [47]. This would be also in agreement for our peptides, since we supposed helix formation for all of our peptides and have observed increased uptake with increased hydrophobicity. In addition, it is known that CF fluorescence is lowered when in acidic compartments. Therefore, in future we will perform careful studies using fluorescence microscopy that will show if those different fluorescent values might depend on different local distributions of the peptides within the cells.

More insights into the mechanism of action

Our results reported thus far let us conclude that the novel AMPs act very fast against bacterial and cancerous cells and presumably by a membrane lysis process. To test the mode of action and the potential of membrane disruption when in contact with mammalian cells, we analyzed the activity of lactate dehydrogenase (LDH) released from HeLa cells (Figure 7), since those cells were most affected after peptide treatment. From the third generation we only included peptides **3d**-**3g**, since they appeared to be the most active ones out of this series. As depicted from Figure 7, we observed high outflow of LDH after 1 h incubation of increasing peptide concentrations of up to 40 µM. This was very prominent and more pronounced when cells were incubated with peptides **4b**-**4e**. Again, **3g** displayed a high membrane activity comparable to the fluorinated peptides. Electrostatic attraction might be the major reason for this activity observed. Indeed, it was already discussed that the interaction between negatively charged components of cancer cells and the positively

charged AMPs plays one major role in the strong binding and selective disruption of cancer cell membranes [48].

FIGURE 7

Lastly, we deduced in more detail the mechanism of action when in contact with bacterial cells. For this we chose to compare peptides **3g** and **4e**, since they were the most active from the respective optimization rounds and comprised different lengths and substitutions.

We used scanning electron microscopy (SEM) to find out about alterations in the morphology of the outer bacterial membrane. Therefore, *B. subtilis*, *C. glutamicum* and *P. fluorescens* were chosen as representatives and incubated for 90 min with 4 x MIC of **3g** and **4e** (Figure 8). As was nicely seen, all bacteria were characterized by a loss of structural integrity after peptide treatment, assumedly due to the peptides inducing antimicrobial effects on the membrane [49]. As the same observation was made for gram-positive and gram-negative bacteria, we concluded that the peptides affected them in a similar way, even though they have different types of cell walls. Essentially, we hypothesized that the novel peptides mainly acted by membrane depolarization and deformation processes leading to membrane disruption and finally cell lysis.

FIGURE 8

Conclusions

The peptides we have created in this work stand out by their greatly enhanced antimicrobial activities compared to the original cell-penetrating peptide sC18. Among all peptides generated, especially **3g** and **4b**-**4e** evolved as interesting candidates for further broad-spectrum AMP development. Notably, first studies demonstrated also activity against pathogenic *P. aeruginosa*. Since quick and direct disruption of the membrane was observed, a bactericidal effect is most likely the way of action for those peptides. That the peptides act by this prompt membrane disintegration, was revealed by investigating their proteolytic stability. Obviously, they were highly prone to degradation, and the resulting fragments were not as active as the longer parent peptides. Indeed, from these observations, it can be hypothesized that the peptides must kill the bacteria quickly before they were inactivated by secreted bacterial proteases. Moreover, preliminary proteome studies revealed no significant changes in protein abundances (data not shown), speaking again in favor of a fast membrane

lysis provoked by the peptides. However, such rapid mechanisms would favorize their future application in topical treatment strategies. This would underpin the application of the peptides as coatings of metallic surfaces that can be used for protheses [50] or clinical devices, minimizing the risk of device infection [51].

Also, we did not note any significantly toxic effects towards hRBCs or, for most of the peptides, even HEK293 cells, pointing to a promising selectivity index. For instance, peptide **4e** exhibited MIC_{50} values below 1 µM to several bacterial strains tested but illustrated toxicity to HEK293 cells in concentrations above 40 µM. In spite of this, the most interesting candidate would probably be peptide **4b**, showing no signs of cytotoxicity at all towards most types of human cells analyzed, while still expressing significant antimicrobial activity. Additionally, as we also detected considerable toxic effects towards cancer cells, again, peptides **3g** and **4c**-**4e**, might be promising to be further evaluated as anticancer peptides. Even though fluorinated peptides **4c**-**4e** showed even stronger antimicrobial potential, they also expressed increased toxicity against mammalian cells, what let us conclude that **4b** might probably be the most favorable candidate for future antibacterial drug development. However, since peptides **4d** and **4e** did also translocate inside cancerous cells, they might additionally be used as versatile cancer-targeting transporters.

The measured cell selectivity might originate from the different membrane (surface) characteristics of the various cell types investigated (bacterial, as well as mammalian). For the lytic effects we propose that hydrophobicity combined with the high content of basic amino acids is one of the major determinants. Importantly, our results demonstrated herein give new insights into the sequence requirements for developing novel AMPs.

To summarize our findings, we have designed highly active antimicrobial peptides with promising selectivity between bacterial and mammalian cells, as well as also between healthy and cancerous cells. Bearing those intriguing properties, they might be an interesting contribution for further research in these fields.

Competing interests

The authors declare that there are no competing interests associated with the manuscript.

Author contributions

M.D., A.R. and I.N. designed the study, performed experiments and analyzed data. J.G., F.N., T.C. and P.H. performed experiments and analyzed data. M.D., F.N., P.H., T.C., B.M. and I.N. wrote the manuscript.

Acknowledgments

We thank A. Hochheiser for help with mass spectrometry. Financial support by the DFG (German Research Foundation, project NE 1419/10-1) is greatly acknowledged by I.N. and M.D.

References

(1) Duschinsky, D. (1910) P. Ehrlich, Anwendung und Wirkung von Salvarsan: Vortrag, gehalten am 8. Dezember 1910 im ärztlichen Fortbildungskurse in Frankfurt a. M.1). *Dtsch. Medizinische Wochenschrift 36*, 2437–2438.

(2) Fleming, A. (1929) ON THE ANTIBACTERIAL ACTION OF CULTURES OF A PENICILLIUM, WITH SPECIAL REFERENCE TO THEIR USE IN THE ISOLATION OF B. INFLUENZAE. *Br. J. Exp. Pathol. 10*, 226–236.

(3) MEENAN, F. O. (1956) The role of antibiotics in dermatology. *J. Ir. Med. Assoc. 38*, 71–73.

(4) Van Den Bogaard, A. E., and Stobberingh, E. E. (1999) Antibiotic usage in animals. Impact on bacterial resistance and public health. *Drugs 58*, 589–607.

(5) Ventola, C. L. (2015) The antibiotic resistance crisis: causes and threats. *Pharmacol. Ther. 40*, 277–283.

(6) Laws, M., Shaaban, A., and Rahman, K. M. (2019) Antibiotic resistance breakers: Current approaches and future directions. *FEMS Microbiol. Rev. 43*, 490–516.

(7) Parnham, M. J., Haber, V. E., Giamarellos-Bourboulis, E. J., Perletti, G., Verleden, G. M., and Vos, R. (2014) Azithromycin: Mechanisms of action and their relevance for clinical applications. *Pharmacol. Ther. 143*, 225–245.

(8) Ilona Hartmane, Iveta Ivdra, Ingmars Mikazans, A. D. (2015) Clinical Efficacy of Ceftriaxone in Cases of Early Forms of Syphilis | RSU. *SPapers / RSU* 17–21.

(9) van Duin, D., and Paterson, D. L. (2016) Multidrug-Resistant Bacteria in the Community: Trends and Lessons Learned. *Infect. Dis. Clin. North Am. 30*, 377–390.

(10) Mahlapuu, M., Håkansson, J., Ringstad, L., and Björn, C. (2016) Antimicrobial peptides: An emerging category of therapeutic agents. *Front. Cell. Infect. Microbiol. 6*, 194.

(11) Derakhshankhah, H., and Jafari, S. (2018) Cell penetrating peptides: A concise review with emphasis on biomedical applications. *Biomed. Pharmacother. 108*, 1090–1096.

(12) Garner, J., and Harding, M. M. (2007) Design and synthesis of α-helical peptides and mimetics. *Org. Biomol. Chem. 5*, 3577–3585.

(13) Bowerman, C. J., and Nilsson, B. L. (2012) Self-assembly of amphipathic β-sheet peptides: insights and applications. *Biopolymers 98*, 169–184.

(14) Dickson, J. S., and Koohmaraie, M. (1989) Cell surface charge characteristics and their relationship to bacterial attachment to meat surfaces. *Appl. Environ. Microbiol. 55*, 832–836.

(15) Lei, J., Sun, L. C., Huang, S., Zhu, C., Li, P., He, J., Mackey, V., Coy, D. H., and He, Q. Y. (2019) The antimicrobial peptides and their potential clinical applications. *Am. J. Transl. Res. 11*, 3919–3931.

(16) Ho, Y. H., Shah, P., Chen, Y. W., and Chen, C. S. (2016) Systematic analysis of intracellular-targeting antimicrobial peptides, bactenecin 7, hybrid of pleurocidin and dermaseptin, proline-arginine-rich peptide, and lactoferricin b, by using Escherichia coli proteome microarrays. *Mol. Cell. Proteomics 15*, 1837–1847.

(17) Liu, G., Yang, F., Li, F., Li, Z., Lang, Y., Shen, B., Wu, Y., Li, W., Harrison, P. L., Strong, P. N., Xie, Y., Miller, K., and Cao, Z. (2018) Therapeutic potential of a scorpion venom-derived antimicrobial peptide and its homologs against antibiotic-resistant Gram-positive bacteria. *Front. Microbiol. 9*, 1159.

(18) Hsieh, I. N., and Hartshorn, K. L. (2016) The role of antimicrobial peptides in influenza virus infection and their potential as antiviral and immunomodulatory therapy. *Pharmaceuticals 9*, 53.

(19) Bondaryk, M., Staniszewska, M., Zielińska, P., and Urbańczyk-Lipkowska, Z. (2017) Natural antimicrobial peptides as inspiration for design of a new generation antifungal compounds. *J. Fungi 3*, 46.

(20) Vizioli, J., and Salzet, M. (2002) Antimicrobial peptides versus parasitic infections? *Trends Parasitol. 18*, 475–6.

(21) Zasloff, M. (1987) Magainins, a class of antimicrobial peptides from Xenopus skin: Isolation, characterization of two active forms, and partial cDNA sequence of a precursor. *Proc. Natl. Acad. Sci. U. S. A. 84*, 5449–5453.

(22) Larrick, J. W., Hirata, M., Shimomoura, Y., Yoshida, M., Zheng, H., Zhong, J., and Wright, S. C. (1993) Antimicrobial activity of rabbit CAP18-derived peptides. *Antimicrob. Agents Chemother. 37*, 2534–2539.

(23) Oliva, R., Chino, M., Pane, K., Pistorio, V., De Santis, A., Pizzo, E., D'Errico, G., Pavone, V., Lombardi, A., Del Vecchio, P., Notomista, E., Nastri, F., and Petraccone, L. (2018) Exploring the role of unnatural amino acids in antimicrobial peptides. *Sci. Rep. 8*, 8888.

(24) Gaspar, D., Salomé Veiga, A., and Castanho, M. A. R. B. (2013) From antimicrobial to anticancer peptides. A review. *Front. Microbiol. 4*, 294.

(25) Feni, L., and Neundorf, I. (2017) The current role of cell-penetrating peptides in cancer therapy. *Adv. Exp. Med. Biol. 1030*, 279–295.

(26) Gabernet, G., Gautschi, D., Müller, A. T., Neuhaus, C. S., Armbrecht, L., Dittrich, P. S., Hiss, J. A., and Schneider, G. (2019) In silico design and optimization of selective membranolytic anticancer peptides. *Sci. Rep. 9*, 11282.

(27) Chen, B., Le, W., Wang, Y., Li, Z., Wang, D., Ren, L., Lin, L., Cui, S., Hu, J. J., Hu, Y., Yang, P., Ewing, R. C., Shi, D., and Cui, Z. (2016) Targeting negative surface charges of cancer cells by multifunctional nanoprobes. *Theranostics 6*, 1887–1898.

(28) Neundorf, I., Rennert, R., Hoyer, J., Schramm, F., Löbner, K., Kitanovic, I., and Wölfl, S. (2009) Fusion of a short HA2-derived peptide sequence to cell-penetrating peptides improves cytosolic uptake, but enhances cytotoxic activity. *Pharmaceuticals 2*, 49–65.

(29) Lützenburg, T., Neundorf, I., and Scholz, M. (2018) Direct carborane-peptide conjugates: Synthesis and evaluation as non-natural lipopeptide mimetics. *Chem. Phys. Lipids 213*, 62–67.

(30) Klimpel, A., and Neundorf, I. (2018) Bifunctional peptide hybrids targeting the matrix of mitochondria. *J. Control. Release 291*, 147–156.

(31) Horn, M., and Neundorf, I. (2018) Design of a novel cell-permeable chimeric peptide to promote wound healing. *Sci. Rep. 8*, 16279.

(32) Neundorf, I. (2019) Antimicrobial and cell-penetrating peptides: How to understand two distinct functions despite similar physicochemical properties, in *Advances in Experimental Medicine and Biology*, pp 93–109. Springer New York LLC.

(33) Chen, Y., Guarnieri, M. T., Vasil, A. I., Vasil, M. L., Mant, C. T., and Hodges, R. S. (2007) Role of peptide hydrophobicity in the mechanism of action of α-helical antimicrobial peptides. *Antimicrob. Agents Chemother. 51*, 1398–1406.

(34) Lyu, Y., Yang, Y., Lyu, X., Dong, N., and Shan, A. (2016) Antimicrobial activity, improved cell selectivity and mode of action of short PMAP-36-derived peptides against bacteria and Candida. *Sci. Rep. 6*, 27258.

(35) Meng, H., and Kumar, K. (2007) Antimicrobial activity and protease stability of peptides containing fluorinated amino acids. *J. Am. Chem. Soc. 129*, 15615–15622.

(36) Hänchen, A., Rausch, S., Landmann, B., Toti, L., Nusser, A., and Süssmuth, R. D. (2013) Alanine Scan of the Peptide Antibiotic Feglymycin: Assessment of Amino Acid Side Chains Contributing to Antimicrobial Activity. *ChemBioChem 14*, 625–632.

(37) Huang, H. W. (2006) Molecular mechanism of antimicrobial peptides: The origin of cooperativity. *Biochim. Biophys. Acta - Biomembr. 1758*, 1292–1302.

(38) Gessner, I., Klimpel, A., Klußmann, M., Neundorf, I., and Mathur, S. (2020) Interdependence of charge and secondary structure on cellular uptake of cell penetrating peptide functionalized silica nanoparticles. *Nanoscale Adv. 2*, 453–462.

(39) Gutsmann, T. (2016) Interaction between antimicrobial peptides and mycobacteria. *Biochim. Biophys. Acta - Biomembr. 1858*, 1034–1043.

(40) Joo, H. S., Fu, C. I., and Otto, M. (2016) Bacterial strategies of resistance to antimicrobial peptides. *Philos. Trans. R. Soc. B Biol. Sci. 371*.

(41) Setty, S. C., Horam, S., Pasupuleti, M., and Haq, W. (2017) Modulating the Antimicrobial Activity of Temporin L Through Introduction of Fluorinated Phenylalanine. *Int. J. Pept. Res. Ther. 23*, 213–225.

(42) Huang, Y., He, L., Li, G., Zhai, N., Jiang, H., and Chen, Y. (2014) Role of helicity of α-helical antimicrobial peptides to improve specificity. *Protein Cell 5*, 631–642.

(43) Carmona, G., Rodriguez, A., Juarez, D., Corzo, G., and Villegas, E. (2013) Improved protease stability of the antimicrobial peptide pin2 substituted with d-Amino acids. *Protein J. 32*, 456–466.

(44) Bacalum, M., and Radu, M. (2015) Cationic antimicrobial peptides cytotoxicity on mammalian cells: An analysis using therapeutic index integrative concept. *Int. J. Pept. Res. Ther. 21*, 47–55.

(45) O'Brien-Simpson, N. M., Hoffmann, R., Chia, C. S. B., and Wade, J. D. (2018) Editorial: Antimicrobial and Anticancer Peptides. *Front. Chem. 6*, 13.

(46) Ruseska, I., and Zimmer, A. (2020) Internalization mechanisms of cell-penetrating peptides. *Beilstein J. Nanotechnol. 11*, 101–123.

(47) Komin, A., Bogorad, M. I., Lin, R., Cui, H., Searson, P. C., and Hristova, K. (2020) A peptide for transcellular cargo delivery: Structure-function relationship and mechanism of action. *J. Control. Release 324*, 633–643.

(48) Hoskin, D. W., and Ramamoorthy, A. (2008) Studies on anticancer activities of antimicrobial peptides. *Biochim. Biophys. Acta - Biomembr. 1778*, 357–375.

(49) Raheem, N., and Straus, S. K. (2019) Mechanisms of Action for Antimicrobial Peptides With Antibacterial and Antibiofilm Functions. *Front. Microbiol. 10*, 2866.

(50) Zhang, B. G. X., Myers, D. E., Wallace, G. G., Brandt, M., and Choong, P. F. M. (2014) Bioactive coatings for orthopaedic implants-recent trends in development of implant coatings. *Int. J. Mol. Sci. 15*, 11878–11921.

(51) Riool, M., de Breij, A., Drijfhout, J. W., Nibbering, P. H., and Zaat, S. A. J. (2017) Antimicrobial peptides in biomedical device manufacturing. *Front. Chem. 5*, 63.

Table 1. Names, amino acid sequences, molecular weights (MW in g/mol), charge and hydrophobicity scores of all synthesized peptides. Hydrophobicity was calculated via the Thermo-Fischer peptide analyzing tool (*http://thermofisher.com*) and hydrophobic moments were determined via heliquest (*https://heliquest.ipmc.cnrs.fr*).

Name	Sequence	MW [g/mol]	Charge	Hydrophobicity	Hydrophobic moment
sC18	GLRKRLRKFRNKIKEK-NH_2	2069.60	+9	19.40	0.555
1a	**I**LRKRLRKFRNKIKEK-NH_2	2125.70	+9	22.63	0.526
1b	G**I**RKRLRKFRNKIKEK-NH_2	2069.60	+9	18.75	0.562
1c	GL**I**KRLRKFRNKIKEK-NH_2	2026.57	+8	28.45	0.585
1d	GLR**I**RLRKFRNKIKEK-NH_2	2054.58	+8	26.48	0.384
1e	GLRK**I**LRKFRNKIKEK-NH_2	2026.57	+8	26.24	0.635
1f	GLRKR**I**RKFRNKIKEK-NH_2	2069.60	+9	19.25	0.561
1g	GLRKRL**I**KFRNKIKEK-NH_2	2026.57	+8	28.81	0.465
1h	GLRKRLR**I**FRNKIKEK-NH_2	2054.58	+8	26.60	0.460
1i	GLRKRLRK**I**RNKIKEK-NH_2	2035.58	+9	17.34	0.556
1j	GLRKRLRKF**I**NKIKEK-NH_2	2026.57	+8	27.23	0.640
1k	GLRKRLRKFR**I**KIKEK-NH_2	2068.65	+9	25.44	0.409
1l	GLRKRLRKFRN**I**IKEK-NH_2	2054.58	+8	26.99	0.579
1m	GLRKRLRKFRNK**I**EK-NH_2	2054.58	+8	26.55	0.525
1n	GLRKRLRKFRNKIK**I**K-NH_2	2053.64	+10	24.94	0.429
1o	GLRKRLRKFRNKIKE**I**-NH_2	2054.58	+8	26.88	0.679
2a	GLRKRLRKF**I**NKIK**I**K-NH_2	2010.61	+9	31.79	0.493
2b	GLRKRLRKF**I**NKIKE**I**-NH_2	2011.55	+7	33.56	0.729
2c	GLRKRLRKFRNKIK**II**-NH_2	2038.63	+9	31.03	0.572
2d	GLRKRLRKF**I**NKIK**II**-NH_2	1995.60	+8	37.00	0.597
3a	GLRKRLRKF**F**NKIKEK-NH_2	2060.59	+8	27.52	0.639
3b	GLRKRLRKFRNKIK**F**K-NH_2	2087.66	+10	27.02	0.429

3c	GLRKRLRKFRNKIKE**F**-NH_2	2088.60	+8	27.66	0.678
3d	GLEKRKRKF**F**NKIK**F**K-NH_2	2078.65	+9	33.42	0.494
3e	GLRKRLRKF**F**NKIKE**F**-NH_2	2079.59	+7	34.59	0.728
3f	GLRKRLRKFRNKIK**FF**-NH_2	2106.66	+9	33.54	0.571
3g	GLRKRLRKF**F**NKIK**FF**-NH_2	2097.65	+8	38,74	0.596
4a	GLRKRLRKFRNKIK**K**-NH_2	1941.39	+10	20.10	0.656
4b	GLRKRLRKF**F**NKIK**F**-NH_2	1951.38	+8	35.09	0.561
4c	GLRKRLRKF**X_1**NKIK**X_1**-NH_2	1987.36	+8	36.93 *	/
4d	GLRKRLRKF**X_2**NKIK**X_2**-NH_2	2023.34	+8	37.23 *	/
4e	GLRKRLRKF**X_3**NKIK**X_3**-NH_2	2131.28	+8	38.28 *	/

* X_1: 4-fluorphenylalanine; ** X_2: 3,5-difluorphenylalanine; *** X_3: 2,3,4,5,6-pentafluorphenylalanine; **** extrapolated by correlation to HPLC retention times.

Table 2. MIC_{50} values [µM] for all peptides tested against seven different bacterial strains. Incubation time was 6 h at 37 °C.

Bacterial strain	*B. subtilis*	*C. glutamicum*	*M. luteus*	*M. Phlei*	*P. fluorescens*	*S. typhimurium*	*E. Coli*
Peptide	**MIC_{50} values [µM]**						
sC18	>25	>25	>25	>25	>25	>25	>25
1j	6.9	8.2	14.2	>25	7.6	4.5	>25
1n	>25	8.6	>25	>25	12.6	6.5	>25
1o	5.9	5.5	18.9	>25	12.6	16.4	>25
2a	3.8	4.9	6.0	>25	7.2	1.7	>25
2b	2.5	5.2	1.3	>25	2.3	2.8	>25
2c	3.6	7.6	5.3	>25	4.5	9.2	>25
2d	2.2	5.3	10.9	>25	8.2	2.1	>25
3a	18	9.7	15.0	5.8	10.1	12.1	>25
3b	23.1	14.3	23.3	9.5	19.2	21.3	>25
3c	18.3	10.5	21.4	10.0	12.1	18.9	>25

3d	11.1	2.1	6.3	3.1	4.3	>25	>25
3e	2.0	4.3	13.2	2.5	6.0	12.4	>25
3f	>25	8.6	13.7	5.5	3.4	23.6	>25
3g	1.5	1.5	3.8	2.0	2.2	10.7	>25
4a	24.4	4.8	> 5.0	>5.0	6.0	>5.0	>50
4b	1.9	1.4	1.2	2.0	1.8	2.8	45
4c	0.8	0.9	1.2	1.0	0.8	2.7	17
4d	1.6	0.7	1.0	1.0	1.1	1.2	10
4e	0.5	0.6	1.0	1.0	0.4	1.0	7.5

Table 3. Selectivity index calculation (CC_{100}/MIC_{100}) using MIC_{100} values of *B. subtilis* (BS) and *P. fluorescens* (PF), and CC_{100} values of *HEK293* cells.

		3d	**3e**	**3f**	**3g**	**4a**	**4b**	**4c**	**4d**	**4e**
MIC_{100} [µM]	*B. subtilis*	> 15	> 15	> 20	> 15	> 5	> 3	> 2	> 2	> 1
	P. fluorescens	> 25	> 25	> 25	> 15	> 5	> 3	> 2	> 3	> 1
CC_{100} [µM]	HEK293	> 40	> 40	> 40	> 40	> 40	> 40	> 40	> 40	> 40
Selectivity index	HEK / BS	2.7	2.7	2	2.7	8	13.3	20	20	40
	HEK / PF	1.6	1.6	1.6	2.7	8	13.3	20	13.3	40

Figure Captions

Figure 1. Antimicrobial activity assay of the generation 1 peptides using three different bacterial strains (**a-c**). Bacteria were incubated for 6 h at 37 °C with various peptide concentrations. *Data represent mean ± SD* of n (number of experiments) ≧ 1 *performed in triplicate.* Negative control (water) was set to 100 % to calculate the relative quantity of living cells. (**d**) Positions Arg10 (**1j**), Glu15 (**1n**) and Lys16 (**1o**) turned out to be important, as can be partly explained by the helical wheel projections (https://heliquest.ipmc.cnrs.fr).

Figure 2. Exemplary antimicrobial activity assay of (**a**) isoleucine peptides (**1j**, **1n**, **1o**, **2a**-**2d**) (**b**) phenylalanine peptides (**3a**-**3g**) and (**c**) fluorinated peptides (**4a**-**4e**) using *B. subtilis* and *P. fluorescens*. Bacteria were incubated for 6 h at 37 °C. *Data represent mean ± SD* of n ≧ 3 *performed in triplicate*. Negative control (water) was set to 100 % to calculate the relative quantity of living cells. Data for further bacterial strains are found in Figures S2-S4.

Figure 3. Enzymatic stability of **4a**, **4b** and **4e** (after incubation with 1:50 (m/m) trypsin). **a**) Cleavage-sites of peptides determined by LC-MS. *N*-terminal and *C*-terminal fragments were identified by their mass signature in ESI-MS. **b**) Antimicrobial activity (6 h, 37 °C incubation) of the identified peptide fragments against *B. subtilis* and *P. fluorescens*. **c**) Antimicrobial assay (6 h, 37 °C incubation) using *B. subtilis* and peptides **4a**, **4b** and **4e** at minimal inhibitory concentration, without (full color) or with preceding 18 h treatment in bacterial cell culture supernatant (dashed). Data represent mean ± SD of n ≧ 3 performed in triplicate. Statistical significance was calculated with *t*-test: ns: $p > 0.05$; ***: $p \leq 0.001$.

Figure 4. Hemolysis assay using peptides of generation 3 (**a**) and generation 4 (**b**). Purified human red blood cells (*hRBCs*) were incubated for 24 h at 37 °C. Negative control was water and positive control 1 % Triton X-100. Data represent mean ± SD of n ≧ 3 performed in triplicate. Statistical significance was calculated with *t*-test: ns: $p > 0.05$; *: $p \leq 0.05$.

Figure 5. Cytotoxicity assays after incubating *HEK293* (**a**), *HeLa* (**b**) and *MCF-7* (**c**) cells for 24 h at 37 °C with peptide solutions of generation 3 (left, green) and generation 4 peptides (right, blue). Negative control (water) was set to 100 % to calculate the relative cell viability. Data represent mean ± SD of n ≧ 3 performed in triplicate. Statistical significance was calculated with *t*-test: ns: $p > 0.05$; *: $p \leq 0.05$; **: $p \leq 0.01$; ***: $p \leq 0.001$.

Figure 6. Cellular uptake of generation 3 (10 µM) (**a**) and generation 4 (5 µM) peptides (**b**) in *HeLa* and *HEK293* cells as determined by flow cytometry (counting 10,000 cells). Data was normalized to sC18 and represent mean ± SD of n ≧ 2 performed in triplicate. Statistical significance was calculated with *t*-test: ns: $p > 0.05$; *: $p \leq 0.05$; **: $p \leq 0.01$; ***: $p \leq 0.001$.

Figure 7. LDH release assay of selected generation 3 peptides (**a**) and generation 4 peptides (**b**) when incubated for 1 h with *HeLa* cells. Data represent mean ± SD of n ≧ 2 performed in triplicate. Statistical significance was calculated with *t*-test: ns: $p > 0.05$; ***: $p \leq 0.001$.

Figure 8. Scanning electron microscopy of *B. subtilis* (**a**), *C. glutamic*um (**b**) and *P. fluorescens* (**c**) after 90 min incubation at 37 °C with control (water) and 4 x MIC_{50} of antimicrobial peptides **3g** and **4e**.

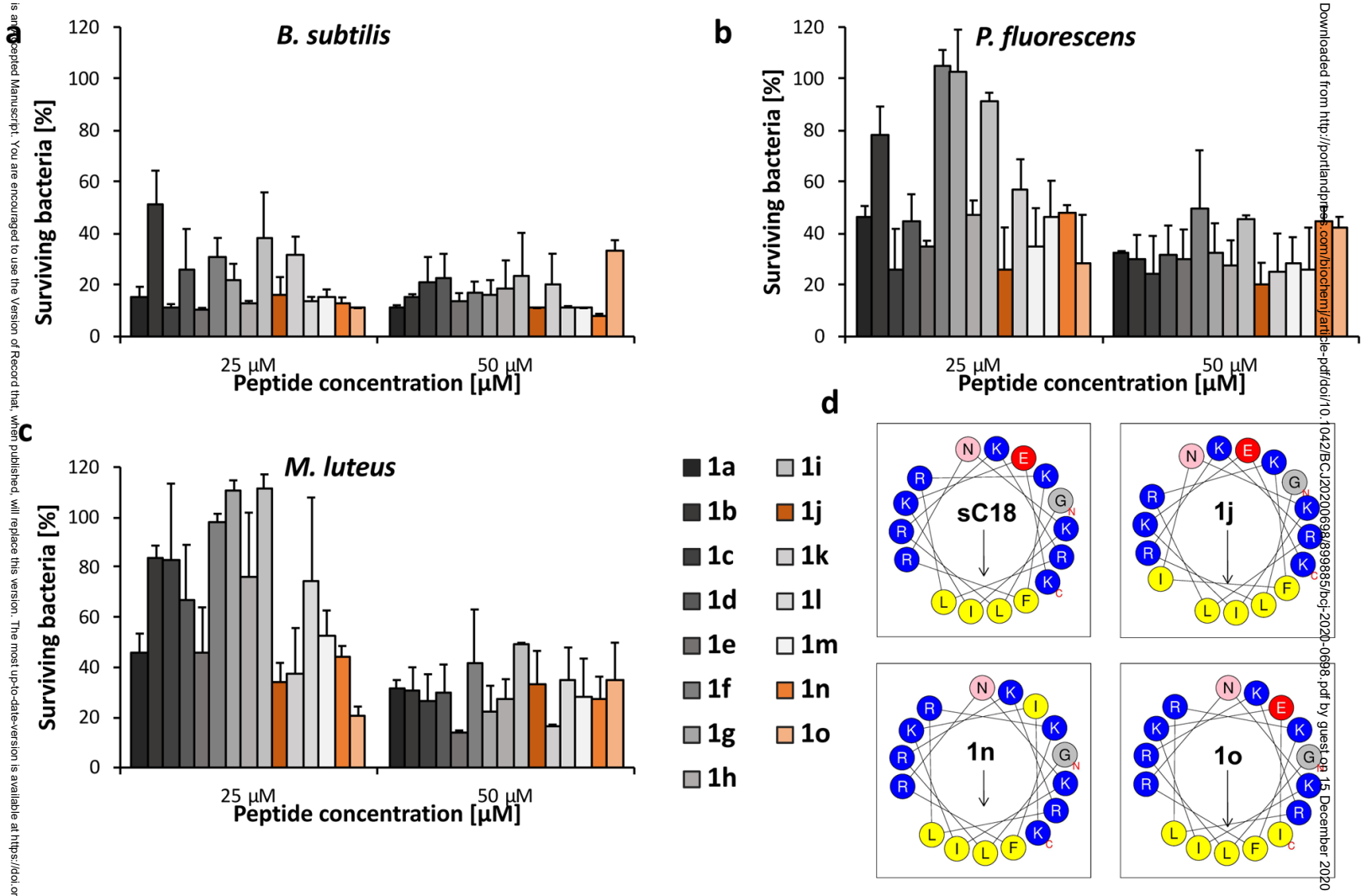

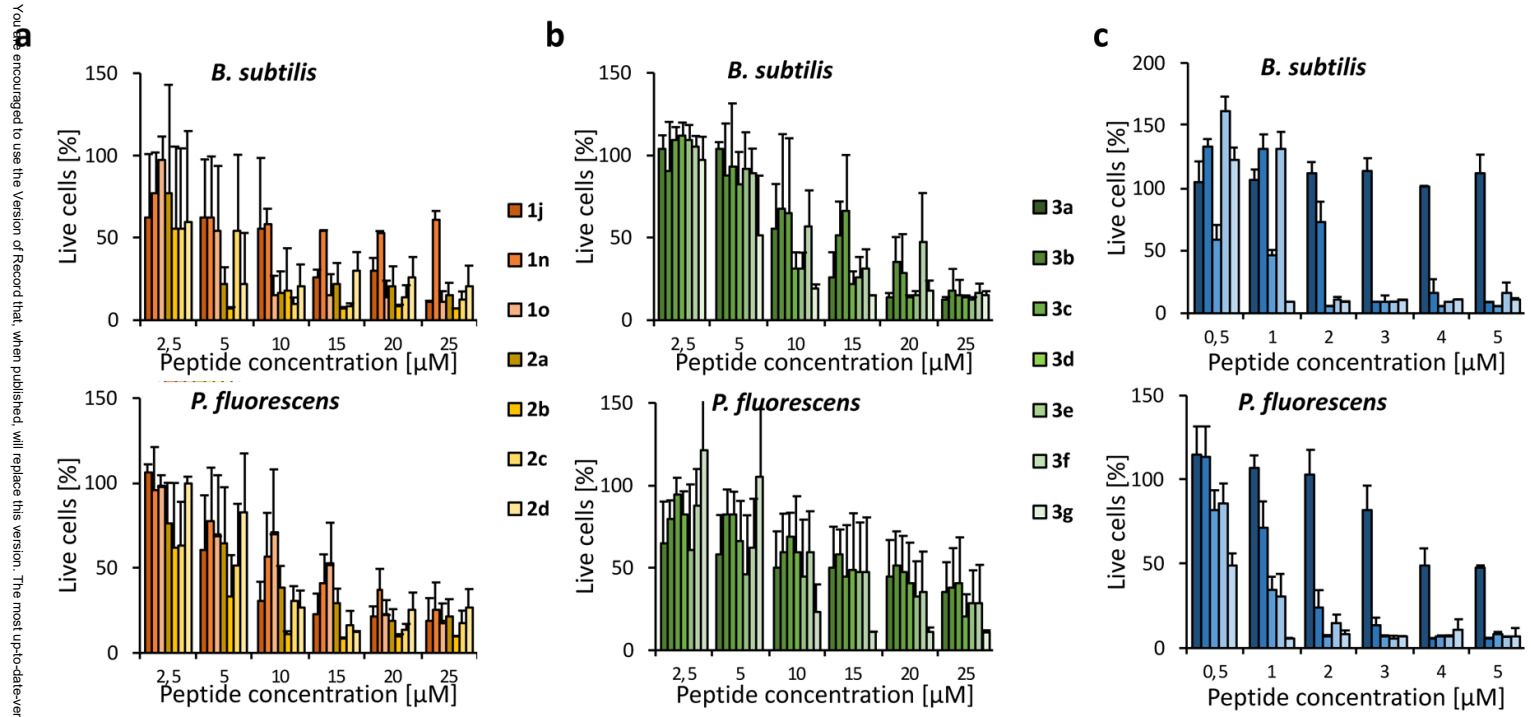

a

Peptide	Cleavage pattern	Time [min]	MW [g/mol]	Fragment A [g/mol]	Fragment B [g/mol]
4a	GLRKR – LRKFRNKIKK	2	1941.6	628.8	1330.8
	LRKFR – NKIKK	5	1330.8	718.9	629.9
4b	GLRKR – LRKFFNKIKF	2	1951.6	628.8	1340.8
	LRKFFNKIK – F	5	1340.8	1193.6	165.2
	LRK – FFNKIK	10	1193.6	415.6	796.0
	FFNK – IK	15	796.0	554.7	259.4
4e	GLRKR – LRKFXNKIKX	2	2131.6	628.8	1520.8
	LRKFXNKIK – X	5	1520.8	1283.6	255.2
	LRK – FXNKIK	10	1283.6	415.6	886.0
	FXNK – IK	60	886.0	644.7	259.4

c

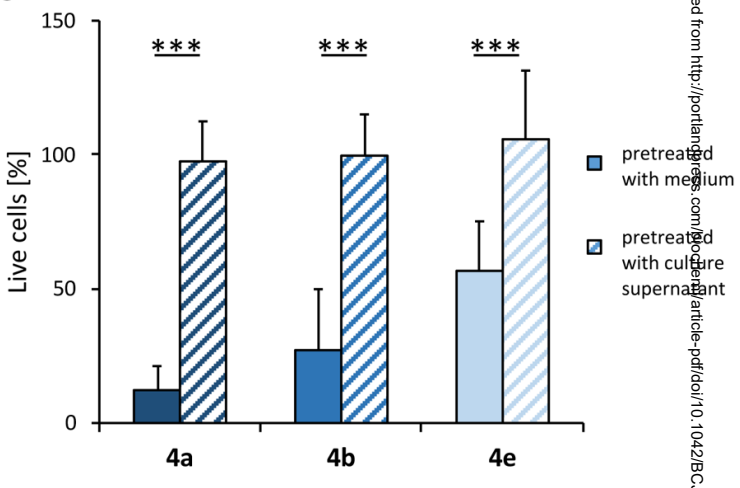

b